Response of a Low Swirl Premixed Flame to Acoustic Perturbations

Mohammad Shahsavari[1,2], Mohammad Farshchi[1], Bing Wang[2], Dan Zhao[3]
[1]Sharif University of Technology, Tehran, Iran
[2]Tsinghua University, Beijing, China
[3]University of Canterbury, Canterbury, New Zealand

Abstract

In this study, large eddy simulations with dynamically thickened flame combustion model are used to study effects of acoustic excitations on low swirl flow and flame features. Obtained results show that external excitations induce perturbations in swirl number upstream of the flame front, which in turn change the coherent structures and the temporal recirculation zone features. Moreover, results show that combination of such changes in the flow field induces heat release fluctuations. The Rayleigh index is calculated at various phases of the excitations to investigate the thermoacoustic couplings. Phase-locked results show that the Rayleigh index is positive at the center of the flame at phase angles of 0° and 180°. However, at phase angles of 90° and 270°, the Rayleigh index can be both positive and negative at the central region. Furthermore, the boundary of the flame experiences both damping and driving processes at all phase angles of the excitations. Finally, low swirl flame transfer function is calculated to further identify effects of the excitations on the flame dynamics.

1 Introduction

Lean premixed low swirl combustion is a novel technology to reduce NOx emissions [1]. In this type of combustion, a premixed flame stabilized aerodynamically without aid of any recirculating flow motion [2, 3]. However, previous investigations showed that although recirculating motions are distinct features of high swirl flows, a temporal weak recirculation zone sometime appears downstream of the low swirl lifted flame, which has no effect on the flame stabilization [4].

It is known that lean premixed combustion is highly susceptible to thermoacoustic instabilities [5]. Such instabilities are compounded in low swirl flames, since they are lifted, which makes them to be highly susceptible to any kind of disturbances. In this light, low swirl flame dynamic under acoustic excitations has been subject of numerous studies in recent years. Majority of these investigations have been carried out using experimental methods to study; mechanisms of thermoacoustic instability in low swirl flames [6-9], effects of hydrogen addition on the flame dynamic [10, 11], effects of exhaust gas recirculation on the flame transfer function [12], and effects of the combustor pressure on the flame response [13]. In addition to above mentioned experimental researches, we have utilized large eddy simulations to examined effects of acoustic excitations on reacting low swirl flow characteristics, more specifically on the temporal recirculating motions [14]. Obtained results showed that external flow excitations increase the strength of the weak recirculation zone. The size of the recirculation zone is at the maximum value, when the flow is excited by the dominant hydrodynamic frequency of the flow

Correspondence to: Mohammad Shahsavari, shahsavari@mail.tsinghua.edu.cn

field [14].

In continuation of our previous efforts to study low swirl flame dynamics under external excitations, the main objective of this paper is to further address effects of the acoustic excitations on both flame and flow features. Moreover, investigations are carried out to evaluate flame dynamics in an acoustically driven environment in terms of calculating Rayleigh index and flame transfer function.

2 Numerical Method

In this paper, large eddy simulation and dynamically thickened flame combustion model are used to study low swirl flame dynamic under acoustic excitations. A dynamic one equation eddy viscosity model [15] is used to model turbulent subgrid-scale contributions. The objective of thickened flame combustion model is to artificially thicken the flame by a factor of F (thickening factor) in order to capture it on a LES grid [16]. However, thickening process causes the flame to be less sensitive to small scale turbulent structures. To counteract this underestimation, an efficiency function should be used to mimic effects of turbulent flow on the flame. Here, the thickening factor and the efficiency function of the combustion model are calculated using dynamic approaches proposed by Strakey [15] and Colin et al. [16], respectively. Here, a two-step reaction mechanism is used to model chemical reactions of CH_4/Air combustion [4]. In this study, second-order schemes are used to discretize temporal, convection and diffusion terms. Pressure-velocity coupling is achieved using the pressure implicit with splitting operators. The present reacting LES solver is developed in the OpenFOAM platform (the open-source CFD toolbox).

3 Computational Domain and Boundary Conditions

The computational domain consists of a cylinder with the diameter of 400 mm and height of 550 mm, which surrounds a low swirl burner with the swirl number of 0.55. The domain is constructed according to the low swirl burner developed at Lund University [17] (figure 1). The inlet boundary is placed at the outlet of the swirler (50 mm inside the burner), through which a lean premixed methane/air mixture with the equivalence ratio of 0.62 is injected through the inlet. Velocity inlet boundary conditions are specified by using the profiles provided by Petersson et al. [17]. Turbulent fluctuations are imposed at the inlet boundary conditions using Kornev et al. method [18]. Outside the burner (at the bottom of the cylinder), an axial co-flow of air with the velocity of 0.3 m/s is placed. A no-slip boundary condition and a far-field boundary condition are used at the burner and combustor side boundaries, respectively. A convective boundary condition is specified at the outflow. In the present study, the inlet velocity boundary condition is perturbed using;

$$\vec{U}(r,t)_{inlet,excited} = \vec{U}(r,t)_{inlet,unexcited}[1 + A\sin(2\pi f t)] \tag{1}$$

where, $\vec{U}(r,t)_{inlet,excited}$ and $\vec{U}(r,t)_{inlet,unexcited}$ are inlet velocity vectors with and without external excitations, respectively. Moreover, A and f denote amplitude and frequency of the forcing function, respectively. Here, amplitude of the excitations is 10% and frequency is chosen in the range of 100-700 Hz.

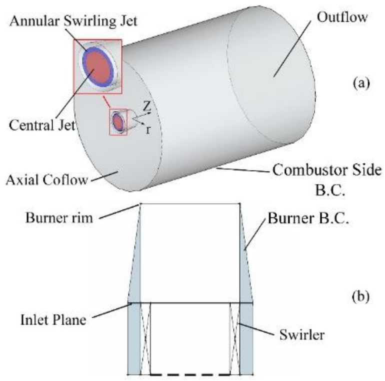

Figure 1. a) Computational domain and boundary conditions, b) side view of the burner

The structured computational mesh consists of 3.4 million hexahedral cells. Cell size is 0.5-1.0 mm in the regions containing the flame and shear layers, which is on the order of Taylor scale of the flow. Close to the burner wall, the grid resolution yields y^+ of 4, which is within the viscous sub-layer. To make sure the numerical results are grid independent, simulations are carried out with 1.6, 2.6 and 4.7 million cells [4]. A set of experimental data from Nogenmyr et al. [19] is used for the validation, including velocity components, temperature and methane concentration. Acceptable agreement is obtained between the numerical and experimental results [4, 14].

4 Results and Discussions

In this section, first, investigation is carried out to demonstrate effects of acoustic excitations on the low swirl flow and flame features. Next, the flame dynamics are studied in more details by calculating the Rayleigh index and flame transfer function.

Figure 2 shows spatial distribution of thickening factor in the present investigation. Results show that the low swirl flame is bowl shape, which is stabilized at a considerable distance downstream of the burner rim. The Zeldovich laminar flame thickness of a methane/air flame at equivalence ratio of 0.65 is 0.14 mm. Based on figure 2, the average value of thickening factor is 18 in the flame front. Therefore, the thickened flame thickness is 2.5 mm. In the present study, the grid size is 0.7 mm near the flame front. Therefore, the flame is captured in 3-4 grids.

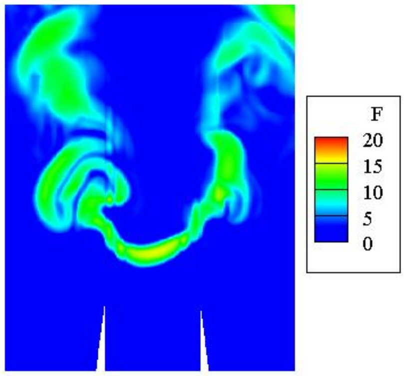

Figure 2. Spatial distribution of thickening factor

Figure 3 summarizes effects of excitations (at forcing frequency of 422 Hz) on the reacting low swirl flow in different phases. Here, heat release fluctuations and flame lift off distance are used to show response of flame to the excitations. Furthermore, fluctuations of the temporal recirculation zone (the reversed flow mass flow oscillations) and swirl number fluctuations are used to evaluate effects of the excitations on the flow field. To such aim, the heat release fluctuations are calculated after integrating heat release over the entire computational domain during the computation. Furthermore, the flame lift off distance is the axial distance between the location of the maximum heat release and the burner rim. Moreover, the reverse flow mass flow rate is calculated as below,

$$M_r = \int_{Z=Z_i}^{Z=Z_e} \int_{r=0}^{r=r_{0,n}} 2\pi r \rho U_z dr dZ \quad (2)$$

where Z_i and Z_e are the axial locations of the first and second stagnation points of the temporal recirculation zone. Furthermore, $r_{0,n}$ is the radial location of the boundary of the recirculation zone. Here, $U_z=0$ is used to discern the boundary of the recirculation zone. Moreover, here, swirl number fluctuation is calculated upstream of the flame front using,

$$S = \frac{\int_0^{r_0} \rho U_z U_r r^2 dr}{R_0 \int_0^{r_0} \rho U_z^2 r dr} \quad (3)$$

where ρ is density, U_z is axial velocity, U_r is radial velocity, r_0 is radius of the computational domain and R_0 is the burner radius.

Results show that responses of both heat release and flame lift off distance fluctuations are in phase with the reference wave. The flame experiences severe fluctuations at phase angle of 90° and 270°, in which the flame has maximum and minimum distance from the burner rim, respectively. On the other hand, the flow field response shows that both the reversed flow and swirl number fluctuations have 180° phase difference with the reference wave.

Figure 4 shows effects of the excitations on the coherent structures of the low swirl jet. Coherent structures of the unexcited case is shown for the reference. As it is expected, such structures are helical type for the unexcited case, since the flow is dominant both by axial and tangential motions. The structures are more ordered near the burner rim. However, they damp rapidly passing the flame, as it is show in previous investigation [14]. The excited case results show that such structures become more ring like under the excitations. Such ring like structures are more ordered at phase angle of 90° and 270°, while at phase angles of 0° and 180°, they are very weak and dispersed. Therefore, it can be concluded that these structures are at play in heat release fluctuations, since as it is shown in figure 3, heat release fluctuations are at maximum value at phase angles of 90° and 270°.

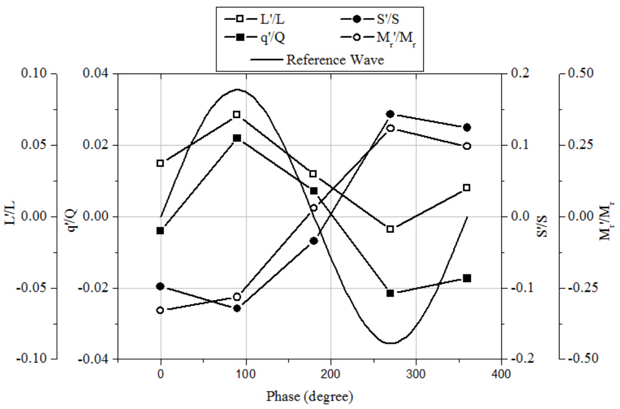

Figure 3. Response of flow and flame features to the acoustic excitations

Figure 4. Coherent structures in unexcited and excited reacting low swirl flows

Above investigations show that external excitations induce perturbations in swirl number above the flame front, which changes the coherent structures and recirculating motions features. On the other hand, acoustic perturbations changes both flame area and speed, which are not shown here. However, combination of all above changes on the low swirl flame induces heat release fluctuations (figure 3).

In an attempt to get more insight into low swirl dynamics under the excitations, Rayleigh index (RI) is calculated at different phases of the excitations. To such aim, first, phase-locked averaging is carried out to calculate spatial distributions of ensemble averaged pressure and heat release fluctuations in each phase of the excitations. Then, the phase-locked averaged data is averaged in the azimuthal direction. Finally, Rayleigh index is calculated based on the azimuthally averaged data. Figure 5 shows spatial distributions of Rayleigh index and boundary of the flame at each phase of the excitations. Here, the flame location in each phase is shown by using 0.1% of the maximum reaction rate in the corresponding case. Results show that the Rayleigh index is always positive at the center of the flame at phase angles of 0° and 180°, while it can be both negative and positive at the corresponding region at phase angles of 90° and 270°. Results also show that boundary of the flame experiences complex damping and driving regions in all phases of the excitations. However, damping and driving regions are more widespread at phase angles of 90° and 270° as compared to phase angles of 0° and 180°. The complex couplings at the boundary of the flame is also observed in experimental investigations carried out by Kang et al. [7]. It was believed that such couplings are a result of shear layer entrainment at the flame boundary [7]. This is the first time numerical simulations reproducing such couplings. Above investigations show that there are different couplings between the excitations and flame. The center of the flame response more coherently to the perturbations as compared to the boundary of the flame. Such response of the flame is highly phase dependence. It is believed that the thermosacoustic coupling at the central region is related to the central flame movement due to the imposed perturbations. However, further investigations are required to make a conclusion.

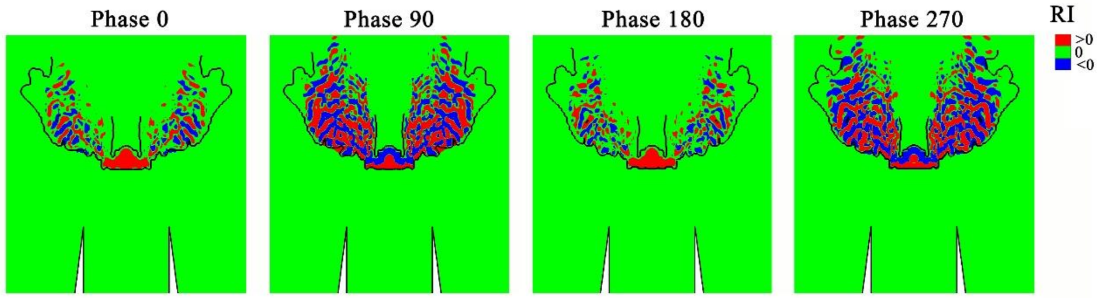

Figure 5. Phase-locked spatial distribution of Rayleigh index

In this section, in order to quantitatively describe the low swirl flame response to the upstream velocity perturbations, the flame transfer function defined as below is calculated by conducting numerical simulations at different forcing frequencies,

$$F(\omega) = Ae^{-\omega\tau} \tag{4}$$

where A is the amplitude and τ is the time lag between heat release fluctuations and forcing waves, which comprises of two parts; convective time scale, which is the time required for the forcing waves to move from the source of the excitations to the flame front, and natural time lag between heat release and velocity (pressure) perturbations at the flame front (figure 6). The amplitude and the natural time lag are obtained by post processing the numerical results at the flame front. To such aim, a probe is located at the flame front to collect velocity perturbations at the flame, while heat release fluctuations are obtained by integrating heat release over the entire computational domain. In the present study, the convective time scale is calculated as below,

$$\tau_c = -\left(\frac{\emptyset(r=0,\theta,Z=flame\ \ location,t=t_{sim})}{\emptyset_{ref}(r=0,\theta,Z=flame\ \ location,t=t_{sim})} - t_{sim}\right) \tag{5}$$

where $\emptyset$ and $\emptyset_{ref}$ are two scalars used to evaluate the convective time scale for the disturbances to go from the inlet boundary condition to the flame front. Furthermore, t_{sim} is the simulation time. Here, scalars are obtained by solving following transport equations during the numerical simulations,

$$\frac{\partial(\bar{\rho}\widetilde{\emptyset})}{\partial t} + \frac{\partial}{\partial x_i}\left(\bar{\rho}\widetilde{U_\iota}\widetilde{\emptyset}\right) = \frac{\partial}{\partial x_i}\left[-\bar{\rho}\overline{D_k}\frac{\partial\widetilde{\emptyset}}{\partial x_i} - \left(-\mu^{SGS}\frac{\partial\widetilde{\emptyset}}{\partial x_i}\right)\right] \tag{6}$$

$$\frac{\partial(\bar{\rho}\widetilde{\emptyset}_{ref})}{\partial t} + \frac{\partial}{\partial x_i}\left(\bar{\rho}\widetilde{U_\iota}\widetilde{\emptyset}_{ref}\right) = \frac{\partial}{\partial x_i}\left[-\bar{\rho}\overline{D_k}\frac{\partial\widetilde{\emptyset}_{ref}}{\partial x_i} - \left(-\mu^{SGS}\frac{\partial\widetilde{\emptyset}_{ref}}{\partial x_i}\right)\right] \tag{7}$$

To such aim, the boundary and initial conditions are set as below,

$$I.C.:\quad \emptyset(r,\theta,Z=0,t=0) = 0 \qquad \& \qquad \emptyset_{ref}(r,\theta,Z=0,t=0) = 0 \tag{8}$$

$$B.C.:\quad \emptyset(r,\theta,Z=0,t=0) = \mathrm{t} \qquad \& \qquad \emptyset_{ref}(r,\theta,Z=0,t=0) = 1 \tag{9}$$

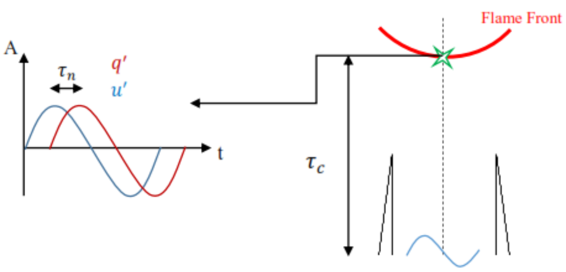

Figure 6. Time lag and convective time scale

Figure 7 shows the amplitude and phase of the flame transfer function for the present low swirl flame. Results show that the flame is more susceptible to the disturbances at low forcing frequencies. In another word, the flame acts as a low pass filter. Moreover, obtained results show that the absolute value of flame response phase increases by increasing the forcing frequency.

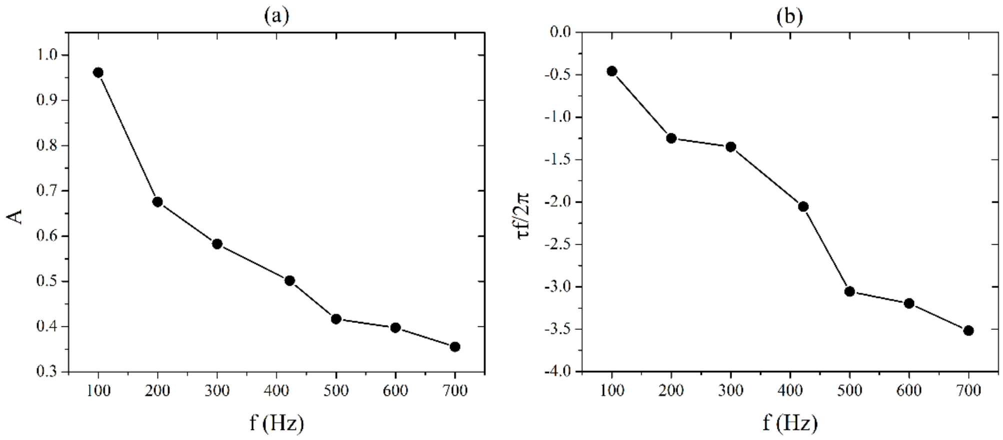

Figure 7. (a) Frequency and (b) phase of the low swirl flame response

5 Conclusions

Dynamics of a reacting low swirl flow under acoustic excitations are studied using large eddy simulations. Results showed that excitations create swirl number fluctuations upstream of the flame front. Moreover, imposed excitations change the coherent structures and the temporal recirculation zone features significantly. Phase-locked Rayleigh index distribution showed that the thermoacoustic coupling at the central region of the flame is highly phase dependence. At phase angles of 0° and 180°, the coupling at the central region is always positive, while at phase angles of 90°and 270°, both damping and driving regions exist simultaneously at the central region of the flame. Obtained results also showed that the boundary of the flame experiences both damping and driving processes in all phases of the excitations. Moreover, calculation of the low swirl flame transfer function showed that the low swirl flame acts as a low pass filter under acoustic excitations.

References

[1] Correa SM (1993). Review of NOx formation under gas turbine conditions. Combust. Sci. Technol. 87: 329.

[2] Cheng RK (1995). Velocity and scalar characteristics of premixed turbulent flames stabilized by weak swirl. Combust. Flame 101:1.

[3] Yegian DT, Cheng RK (1998). Development of a lean premixed low-swirl burner for low NO_X practical applications. Combust. Sci. Technol. 139: 207.

[4]. Shahsavari M, Farshchi M, Arabnejad MH (2017). Large eddy simulations of unconfined non-reacting and reacting turbulent low swirl jets. Flow Turbul. Combust. 98: 817.

[5] Lieuwen T, Torres H, Johnson C, Zinn BT (2001). A mechanism of combustion instability in lean premixed gas turbine combustors. J. Eng. Gas Turb. Power 123: 182.

[6] Shahsavari M, Aravind IB, Chakravarthy SR, Farshchi M (2016). Experimental study of lean premixed low swirl flame under acoustic excitations. International Symposium: Thermoacoustic Instabilities in Gas Turbines and Rocket Engines: Industry Meets Academia GTRE 029.

[7] Kang DM, Culick FEC, Ratner A (2007). Combustion dynamics of a low-swirl combustor. Combust. Flame 151: 412.

[8] Huang Y, Ratner A (2009). Experimental investigation of thermoacoustic coupling for low-swirl lean premixed flames. J. Propuls. Power 25: 365.

[9] Bagheri-sadeghi N, Shahsavari M, Farshchi M (2013). Experimental characterization of response of lean premixed low-swirl flames to acoustic excitations. Int. J. Spray Combust. Dyn. 5: 309.

[10] Yilmaz I, Ratner A, Ilbas M, Huang A (2010). Experimental investigation of thermoacoustic coupling using blended hydrogen-methane fuels in a low swirl burner. Int. J. Hydrogen Energy 35: 329.

[11] Davis DW, Therkelsen PL, Littlejohn D, Cheng RK (2013). Effects of Hydrogen on the thermo-acoustics coupling mechanisms of low-swirl injector flames in a model gas turbine combustor. Proc. Combust. Inst. 34: 3135.

[12] Ranalli J, Ferguson D, (2012). Measurement of flame frequency response functions under exhaust gas recirculation conditions. J. Eng. Gas Turb. Power 134: 1.

[13] Zhang J, Ratner A (2017). Effect of pressure variation on acoustically perturbed swirling flames. Proc. Combust. Inst. 36: 3881.

[14] Shahsavari M, Farshchi M (2018). Large eddy simulation of low swirl flames under external flow excitations. Flow Turbul. Combust. 100: 249.

[15] Strakey PA, Eggenspieler G (2010). Development and validation of a thickened flame modeling approach for large eddy simulation of premixed combustion. J. Eng. Gas Turb. Power 132: 1-9.

[16] Colin O, Ducros F, Veynante D, Poinsot T (2000). A thickened flame model for large eddy simulations of turbulent premixed combustion. Phys. Fluids 12: 1843.

[17] Petersson P, Olofsson J, Brackman C, Seyfried H, Zetterberg J, Richter M (2007). Simultaneous PIV/OH-PLIF, Rayleigh Thermometry/OH-PLIF and Stereo PIV Measurements in a low-swirl flame. 46: 3928.

[18] Kornev N, Kroger H, Turnow J, Hassel E (2007). Synthesis of artificial turbulent fields with prescribed second-order statistics using the random-spot method. Prog. App. Math. Mech. 7: 2100047.

[19] Nogenmyr KJ, Fureby C, Bai XS, Petersson P, Collin R, Linne M (2009). Large eddy simulation and laser diagnostic studies on a low swirl stratified premixed flame. Combust. Flame 156:25.